Kapal: Jurnal Ilmu Pengetahuan dan Teknologi Kelautan
(Kapal: Journal of Marine Science and Technology)
journal homepage : http://ejournal.undip.ac.id/index.php/kapal
2301-9069 (e)
1829-8370 (p)

Benchmark Study of FINE™/Marine CFD Code for the Calculation of Ship Resistance

Ahmad Firdhaus[1)], I Ketut Suastika[2)], Kiryanto[3)], Samuel[3)]

[1]Department of Systems and Naval Mechatronic Engineering, National Cheng Kung University, Taiwan
[2]Department of Naval Architecture, Faculty of Marine Technology, Institut Teknologi Sepuluh Nopember, Surabaya, Indonesia
[3]Department of Naval Architecture, Faculty of Engineering, Universitas Diponegoro, Semarang, Indonesia
[*)] Corresponding Author: ahmdfrds2@gmail.com

Article Info

Keywords:
Benchmarking tests;
CFD code;
FINE™/Marine;
Volume of fluid method;
Ship resistance;

Article history:
Received: 01/07/2021
Last revised: 14/07/2021
Accepted: 15/07/2021
Available online: 15/07/2021
Published: 16/07/2021

DOI:
https://doi.org/10.14710/kapal.v18i2.39727

Abstract

Benchmarking tests are commonly carried out to verify the accuracy of a CFD code, e.g., testing turbulence models, numerical schemes, or implementation of boundary conditions. In this study, benchmarking tests of FINE™/Marine CFD code was done to verify ship resistance calculations' results by comparing them with available experimental data and results of earlier numerical studies. The FINE™/Marine CFD code solves the Reynolds-averaged Navier-Stokes (RANS) equations with appropriate boundary conditions, including modeling of free surface effects. The flow around the DTMB 5415 hull was considered, which advanced in calm water at Fr = 0.248. Simulation results show that the predicted wave contours are consistent with the experimental data. Further, the wave contours and calculated pressure distribution on the hull surface are in good agreement with the results of earlier numerical studies. The total friction, viscous pressure, and wave-making resistance coefficients denoted as C_T, C_F, C_{VP}, and C_W, respectively, are in fairly good agreement with the experimental data and the results of earlier numerical studies.

1. Introduction

Computational fluid dynamics (CFD) have been widely used to study various physical phenomena. Some examples are the study of heat transfers, aerodynamics, and hydrodynamics. While these areas appear different, their main characteristics are almost identical, thus lending themselves to standard solution procedures. Another area of similarity is their inherent tendency to require large amounts of computational effort. Because realistic CFD simulations usually demand the use of fine three-dimensional computational grids incorporating many hundreds of thousands, or even millions, of cells. In addition, compressible flows with heat transfers generally involve at least seven flow variables. If reactive or multi-phase flows are being simulated, the number of variables involved can increase significantly. While funds to purchase appropriate calculation instruments are limited, the computing demand continues to increase. Scientists and engineers are often forced to decide what instruments to give maximum results while offering the best value for their money.

The importance of CFD as a primary tool for analyzing and designing fluid dynamics problems nowadays is unquestionable. In its present state, CFD is at the same level as the state of the art of an experimental approach or a theoretical analysis. To ensure the accuracy and applicability of a CFD code, it is essential to test and verify its results by conducting benchmarking tests. Benchmarking tests can be used, for example, to test new codes for the turbulence models, to conduct grid independence tests, to test different numerical schemes, or to test different boundary conditions.

In ship hydrodynamics, potential and viscous flow models are often used to simulate and examine the flows around ships. Potential flow codes based on the boundary element method are commonly used to study the generation of waves at the free surface [1, 2]. Available potential flow codes usually utilized the Rankine source method to analyze the interactions between ship hulls and the incoming sea waves or to simulate wave resistance problems [3]. In addition, free-surface problems, such as the calculation of wave-making resistance, can also be simulated utilizing viscous flow codes. Two major approaches are widely applied to the free surface computations in these codes, namely, the so-called interface-tracking method, e.g., a moving mesh [4], and the interface-capturing method, e.g., the volume of fluid method (VoF) [5].

Table 1. Principal dimension of the DTMB 5415[6]

Principal Dimension	Full Scale
LPP	142 m
LWL	142.218 m
B	19.06 m
T	6.15 m
Fr	0.248
C_B	0.507
Displacement	8424.4 m^3

Table 2. Test condition for the DTMB 5415 model scale by INSEAN [7, 8]

Principal Dimension	INSEAN Scale 1:24.830
LPP	5.719 m
LWL	5.726 m
B	0.768 m
T	0.248 m
Fr	0.248
C_B	0.507
Displacement	0.554 m^3

This study aims to benchmark tests of the FINE™/Marine CFD code following procedures and guidelines recommended by the International Towing Tank Conference (ITTC) [9].For that purpose, the free-surface flow around the bare hull of the DTMB (David Taylor Model Basin) 5415 ship was simulated utilizing the FINE™/Marine CFD code. The DTMB 5415, designed in the 1980s, was a preliminary design of a Navy surface combatant [6]. The 22nd ITTC Conference has recommended the DTMB 5415 combatant as a benchmark case for CFD computations of ship resistance and propulsion [10]. The principal dimensions of the DTMB 5415 are tabulated in Table 1. Furthermore, Table 2. tabulated the DTMB 5415 model tests condition, performed by the David Taylor Model Basin in Washington D.C. and the Instituto Nazionale per Studied Esperienze di Architettura Navale (INSEAN) in Rome, Italy [7, 8] . The benchmark was done by comparing the FINE™/Marine CFD results with experimental data [11-14] and numerical results from earlier studies [15, 16] available in the literature.

2. Methods

2.1. FINE™/Marine free-surface flow solver

The FINE™/Marine CFD code solves the incompressible Reynolds-averaged Navier Stokes (RANS) equations. The solver applied a finite volume method for the spatial discretization and the discretization of the transport equations. Considering an incompressible multi-phase flow of viscous fluid under isothermal conditions, the mass, momentum, and volume fraction conservation equations are represented in Equations (1-3) as follows:

$$\frac{\partial}{\partial t}\int_v \rho\, dV + \int_S \rho(\mathbf{U}-\mathbf{U}_d).\mathbf{n}\, dS = 0 \tag{1}$$

$$\frac{\partial}{\partial t}\int_v \rho\, U_i dV + \int_S \rho U_i(\mathbf{U}-\mathbf{U_d}).\boldsymbol{n}\, dS = \int_S (\tau_{ij} I_j - pI_i).\mathbf{n}\, dS + \int_S \rho g_i\, dV \tag{2}$$

$$\frac{\partial}{\partial t}\int_v c_i\, dV + \int_S c_i(\mathbf{U}-\mathbf{U}_d).\mathbf{n}\, dS = 0 \tag{3}$$

In Equations (1-3), V is the domain of interest, or a control volume, bounded by a closed surface S moving at the velocity $\mathbf{U}_d$ with a unit normal vector $\mathbf{n}$ directed outward. $\mathbf{U}$ and p represent, respectively, the velocity and pressure fields. Further, τ_{ij} and g_i are the components of the viscous stress tensor and the gravity vector, whereas I_j is a vector whose components vanish, except for the j component, which is equal to unity. c_i is the i-th volume fraction for fluid i and is used to distinguish the presence ($c_i = 1$) or the absence ($c_i = 0$) of fluid i.

The two-equation k-ω SST turbulence model (SST stands for shear stress transport) was applied in the present study [17]. This turbulence model combines the k-ω model for the flow in the inner boundary layer and the k-ε model for the flow in the outer region of and outside of the boundary layer. The transport equations for the SST k-ω model are as follows:

$$\frac{\partial}{\partial t}(\rho k) + \frac{\partial}{\partial x_i}(\rho k u_i) = \frac{\partial}{\partial x_j}\left(\Gamma_k \frac{\partial_k}{\partial x_j}\right) + G_k - Y_k \tag{4}$$

$$\frac{\partial}{\partial t}(\rho \omega) + \frac{\partial}{\partial x_i}(\rho \omega u_i) = \frac{\partial}{\partial x_j}\left(\Gamma_\omega \frac{\partial_\omega}{\partial x_j}\right) + G_\omega - Y_\omega + D_\omega \tag{5}$$

In Equations (4-5), G_k represents the generation of turbulence kinetic energy due to mean velocity gradients, while G_ω Represents the generation of ω. Y_k and Y_ω Represent the dissipation of k and ω due to turbulence, respectively. Further, Γ_k and Γ_ω represent the effective diffusivity of k and ω, respectively, while D_ω Represents the cross-diffusion term. This turbulence model gives accurate predictions of the onset and the amount of flow separation [18].

An interface capturing technique, i.e., the VoF method [19] approach, was used to model the free surface. The water-to-air interface was recovered from the volume fraction [20]. The VoF method defines a scalar field α representing the volume fraction of water in a cell. This field is equal to 1 when the cell is fully occupied by water and equals 0 when the cell is full of air. Cells on the interface have a value of α in the range between 0 and 1, $0 < \alpha < 1$. The fluid properties are defined with interpolation between water and air using α as weight [21] as follows:

$$\rho = a\rho_{water} + (1 - a)\rho_{air} \tag{6}$$

$$\mu = a\mu_{water} + (1 - a)\mu_{air} \tag{7}$$

The VoF field is advected by the velocity field **U**, given by the following equation:

$$\frac{\partial a}{\partial t} + \nabla(\boldsymbol{U}a) = 0 \tag{8}$$

Equations (6-8) are the equations for the two-phase VoF solvers implemented in the ISIS-CFD flow solver. It was developed by the EMN (Equipe Modélisation Numérique) [22]. The solver utilizes a finite volume method to build the spatial discretization of the transport equations. The face-based method is generalized to two-dimensional, rotationally symmetric, or three-dimensional unstructured meshes for which an arbitrary number of consecutive faces bounds non-overlapping control volumes. The flow solver can deal with multi-phase flows and moving grids.

The velocity field is obtained from the momentum conservation equations, and the pressure field is extracted from the mass conservation equation, or continuity equation, transformed into a pressure equation. In turbulent flows, additional transport equations for modeled variables are solved in a form similar to that of the momentum equations, and they can be discretized and solved using the same principles. Incompressible and non-miscible flow phases are modeled through conservation equations for each volume fraction of the phase.

2.2. Geometrical modeling, meshing, and boundary conditions

Figure 1. shows a 3-D CAD model of the DTMB 5415 hull form. To ensure that the numerical model represents the prototype accurately, the hydrostatic characteristics of the model were verified using those of the prototype [23]. Table 3. summarizes the verification results, showing that the differences between model and prototype for all parameters considered are less than 3%, indicating accurate geometrical modeling results.

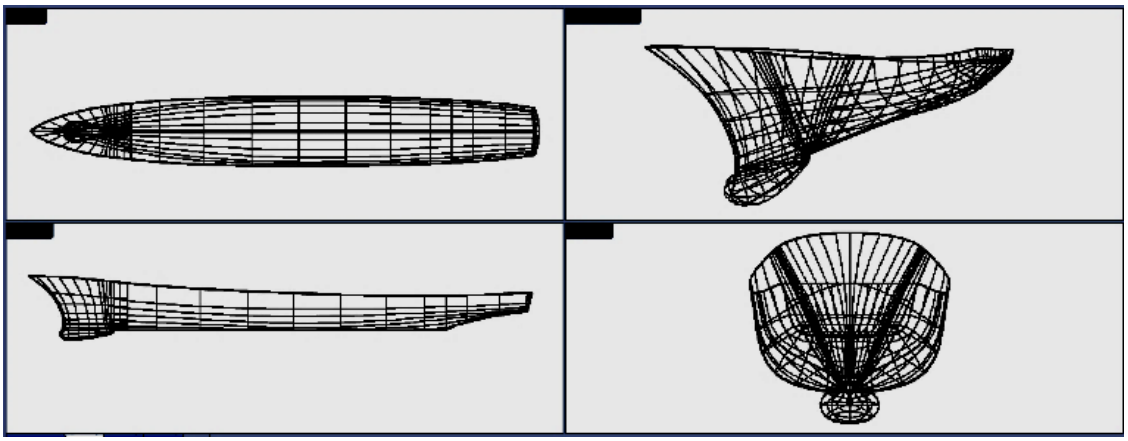

Figure 1. A 3-D CAD model of the DTMB 5415 hull form

Table 3. Comparison of the ship hydrostatic characteristics between the prototype and the 3-D numerical model

Parameter	Prototype (DTMB 5415)	CFD model (Present study)	Percent error [%]
Displacement [ton]	8424.4	8520.0	1.13
Wetted surface area WSA [m^2]	2972.6	3055.0	2.77
Block coefficient C_B	0.507	0.510	0.59
Midship coefficient C_M	0.821	0.820	-0.12

Figures 2 show a mesh of the computational domain with the DTMB 5415 model in it. The mesh was generated using the FINE^{TM}/Marine plugins called C-Wizard [24] and HEXPRESS, the NUMECA grid generator. The C-Wizard plugin guides the users through the process of configuring the mesh and solver parameters. The domain is constructed by defining a box around the ship, and the size of the computational domain is based on the ship's length. Due to symmetry, only half of the ship was simulated.

The boundary conditions of the computational domain as seen on Figure 2. are as follows [25]. The inlet was located at 1.0 *L* upstream from the vessel. The outlet was located at 3.0 L behind the vessel. The sidewall was located at 1.5 *L* aside from the vessel, where *L* is overall at the waterline. The boundary conditions at the inlet, outlet, and sidewall were all prescribed as free stream far-field velocity. The bottom and top walls were located at 1.50 *L* below the vessel and 1.0 *L* above the vessel, respectively, where the boundary conditions were defined as prescribed pressure. The boundary condition on the ship hull was prescribed as no-slip, where a wall function was utilized. Further, the heave and pitch motions were resolved in the simulations.

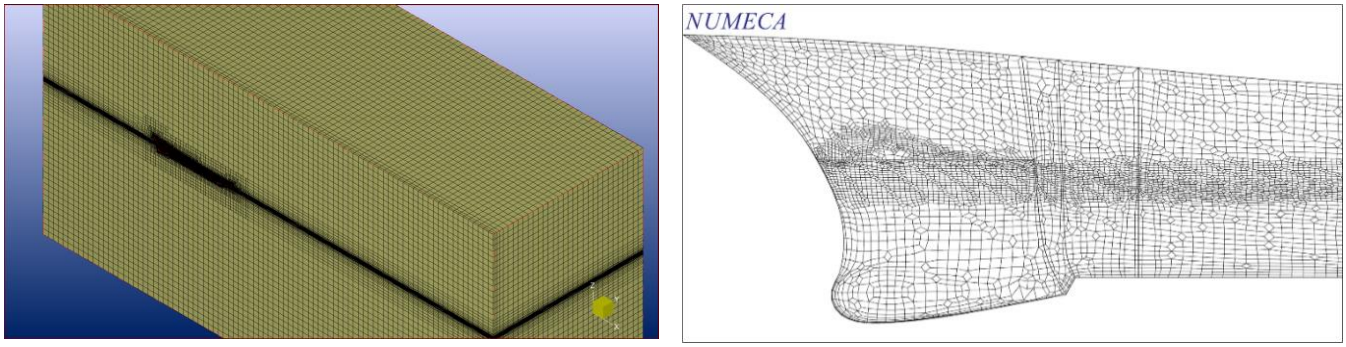

Figure 2. Computational domain with the ship model in it (left) and mesh of the DTMB 5415 hull form, zoomed in near the bow (right)

2.3. Grid independence tests

To determine the optimum grid size (number of cells) and to investigate the convergence of the numerical solution, tests were carried out such that the numerical results complied with the grid-independence criterion [26]. In these tests, the coefficient of total ship resistance C_T was calculated using an increasing number of cells in the simulations. The number of cells in the latter simulation of two subsequent simulations was approximately twice that of the former. A percent error was defined to quantify the difference in C_T between the latter and former simulations. The results are tabulated in Table 4. and plotted in Figure 3.

Table 4. and Figure 3.Figure 3. Coefficient of total ship resistance C_T as function number of cells used in the simulation show that the value of C_T decreases monotonically with an increasing number of cells in the simulations, which is expected to reach an asymptotic value as the number of cells tends to infinity. The number of cells of 3,436,188 ≈ 3.4×10^6 (run number 5) is considered as the optimum number of cells with a percent error of 0.728%, which is much smaller than 2% as recommended in the literature [26].

Table 4. Coefficient of total ship resistance C_T calculated using an increasing number of cells in the simulation

Run number *n*	Number of cells *N*	C_T	Percent error [%]
1	284001	4.56×10^{-3}	
2	448560	4.36×10^{-3}	-4.397
3	980384	4.19×10^{-3}	-3.905
4	1443101	4.15×10^{-3}	-0.954
5	3436188	4.12×10^{-3}	-0.728
6	6908848	4.11×10^{-3}	-0.243

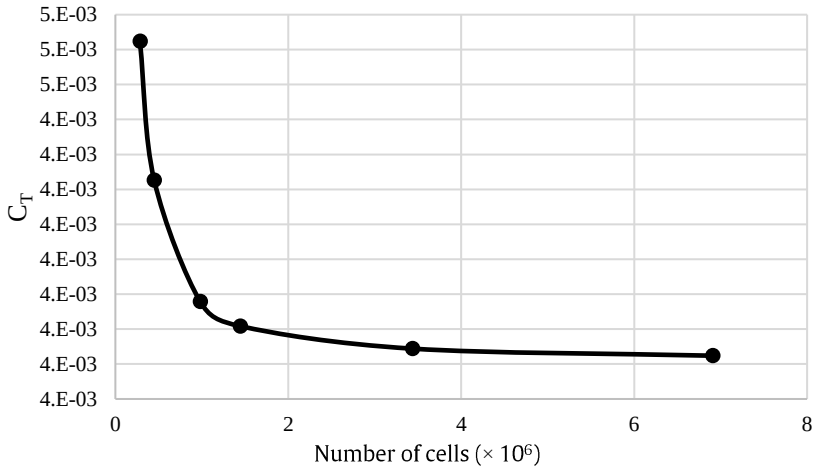

Figure 3. Coefficient of total ship resistance C_T as function number of cells used in the simulation

3. Results and Discussion

Figure 4. shows comparisons of wave contours at *Fr* = 0.248 obtained from the experiments reported by Larsson [12], the numerical results obtained by Ahmed and Soares [15], and from the present study. Figure 4. shows that the wave contours from the present study are consistent with the experimental data and the numerical results from Ahmed and Soares [15].

To explore the details of the wave contours, Figure 5. shows plots of the wave elevation along a line parallel to the ship (y/L = 0.324) obtained from experiments [11], the numerical results by Ahmed and Soares [15], and from the present study. Figure 5. shows that the results from the present study are consistent with the experimental results and are in good agreement with the numerical results of Ahmed and Soares [15].

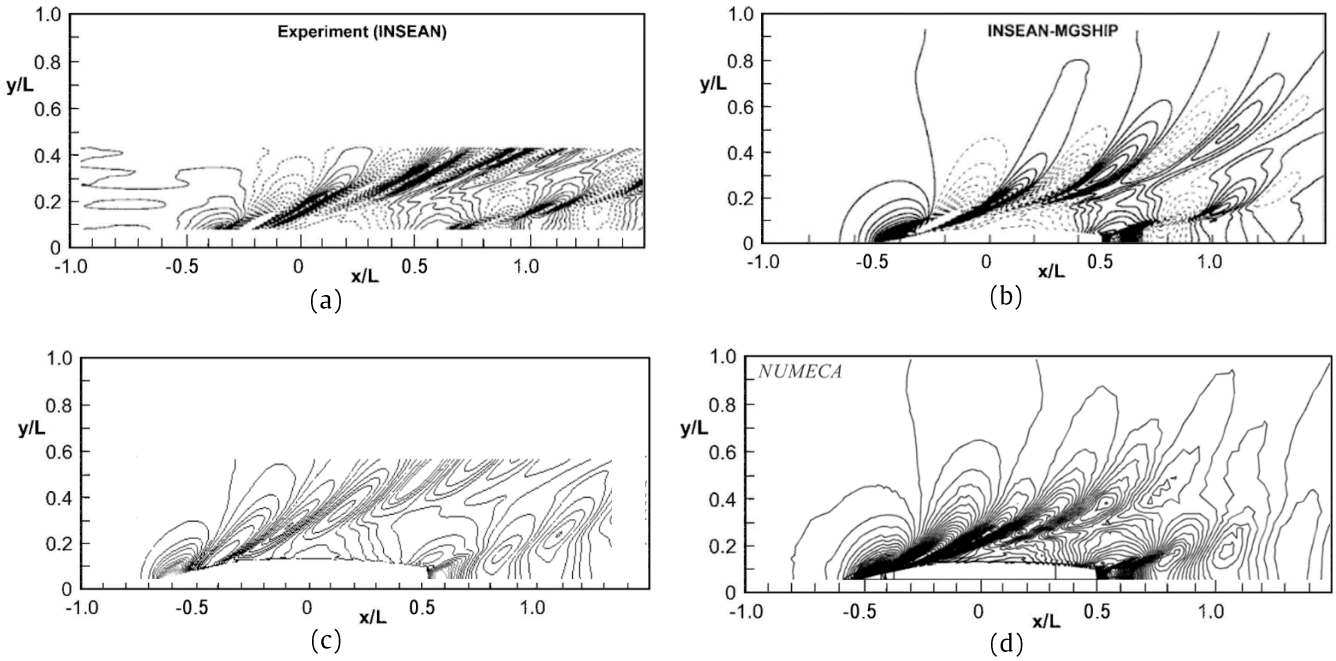

Figure 4. Wave contours at Fr = 0.248: (a) Experiments [12]; (b) predicted using INSEAN-MGSHIP [12]; (c) predicted from [15]; (d) predicted from present study

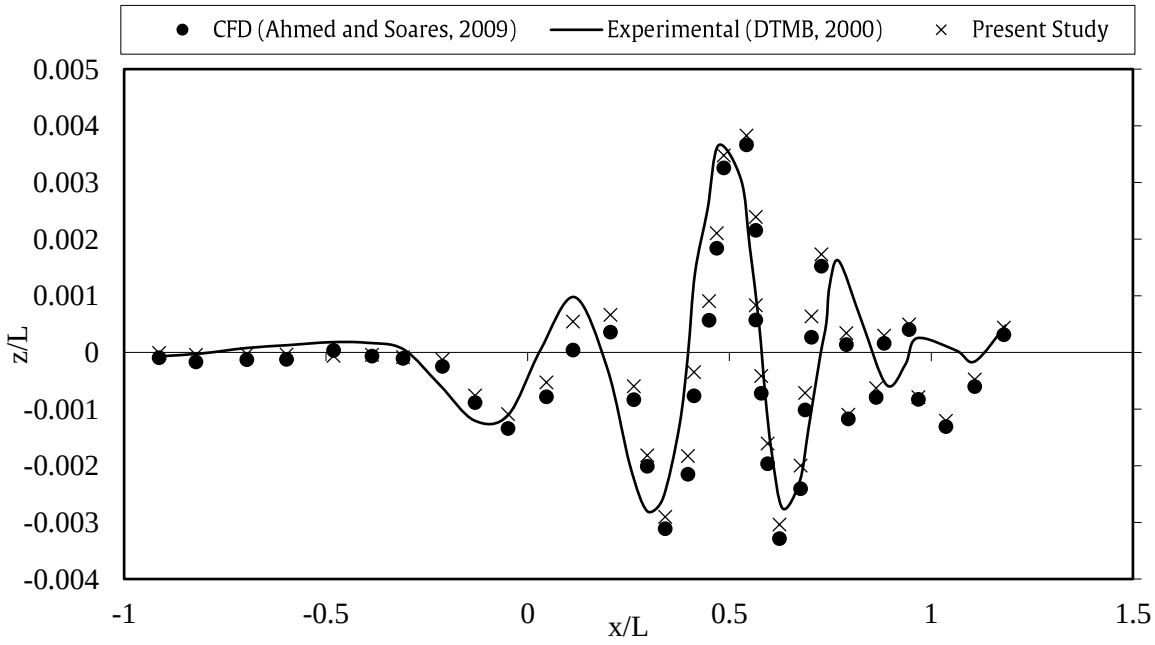

Figure 5. Water elevation along y/L=0.324 at Fr = 0.248 obtained from experiments [11], Ahmed and Soares [15], and the present study

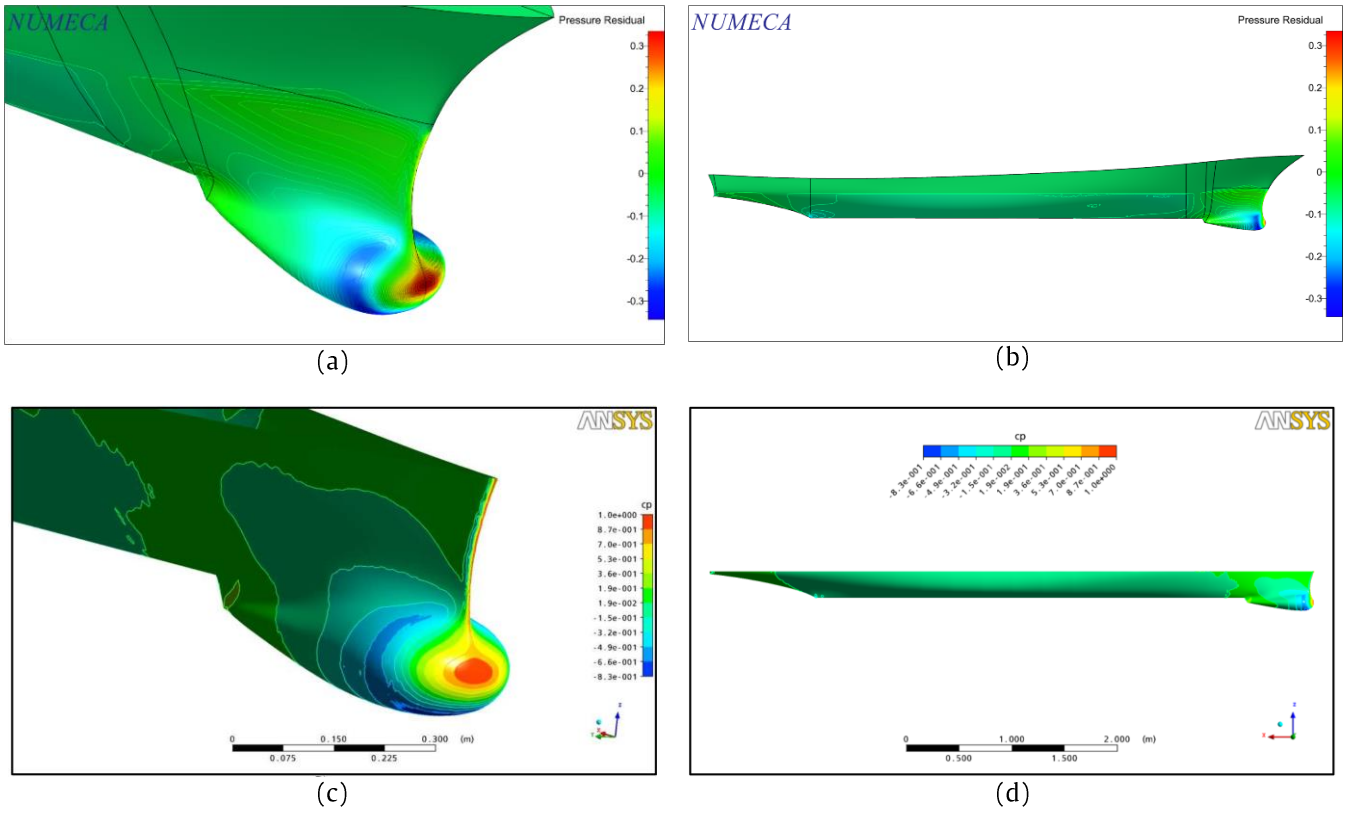

Figure 6. Pressure distribution on the hull surface at Fr = 0.248: (a, b) Present study utilizing FINE™/Marine and (c, d) Reported by Ahmed and Soares [15]

Figure 6(a) and (b) show the pressure distribution on the hull surface of the DTMB 5415 at Fr = 0.248 calculated using FINE™/ Marine. In contrast, Figure 6(c) and (d) show the pressure distribution reported by Ahmed and Soares calculated using Ansys CFX [15]. A high-pressure region is observed in the bow and sonar dome due to the stagnation pressure. At the bow and the sonar dome, the pressure decreased aft from the stagnation region, and the presence of a low-pressure region is observed. This correlates with the increase of fluid velocity in this region due to the curvature of the hull geometry.

Further downstream from the bow region, the pressure increases again due to the effect of hull geometry. Downstream of this position, the pressure decreases slightly again and extends over the entire region of the hull midpart due to nearly the constant cross-section shape in this part of the hull. Figure 6. shows that the calculated pressure distribution from the present study is in good agreement with that reported by Ahmed and Soares [15].

To gain more insight into the ship resistance, it is helpful to decompose the total ship resistance coefficient C_T into friction C_F, viscous pressure C_{VP}, and wave-making resistance coefficients (C_W). In this regard, Hughes [27] introduced a method for the ship-model correlation where the total resistance is assumed as the sum of friction resistance, form resistance, and wave resistance. The values of C_F is calculated from the ITTC 1957 formula (Equation 9), and C_W is calculated from Equation (10) as follows:

$$C_F = \frac{0.075}{(\log_{10} \mathrm{Re} - 2)^2} \tag{9}$$

$$C_W = C_T - C_F(1 + k) \tag{10}$$

Further, the viscous-pressure resistance coefficient C_{VP} is calculated from the following relation:

$$C_{VP} = kC_F \tag{11}$$

The form factor $(1 + k)$ was determined utilizing Prohaska method [28], resulting in $(1 + k) \approx 1.15$ or $k \approx 0.15$ [29].

Table 5 summarizes the values of C_T, C_F, C_{VP}, and C_W from experiments [13], earlier numerical studies by Ahmed and Soares[15], Ahmed et al. [16] and the present study. Table 5 shows that the C_T and C_W obtained in this study are approximately 1.89% and 12.09% smaller than those obtained from the experiments [13], and 3.49% and 13.04% smaller than those reported by Ahmed et al. [16]. The C_F and C_{VP} are in better agreement with the results from the experiments and the numerical study by Ahmed and Soares [15] than the C_T and C_W.

The benchmark reported in this study considers the calculation of ship resistance at a relatively low Froude number, namely Fr = 0.248. A benchmark study of high-speed crafts is recommended for future research, especially at Froude numbers $Fr > 1$. A phenomenon such as the so-called numerical ventilation should be considered [30]. When the speed increases, the volume of air diffused below the ship's hull also increases due to the expected high trim of the vessel.

Table 5. Comparison between experimental and numerical resistance components of the DTMB model 5415

Resistance coefficients	Experiment [13]	CFD			Percentage Error	
		Ahmed and Soares [15]	Ahmed et al. [16]	Present Study	Experiment	Numeric
C_T	4.23×10^{-3}	4.33×10^{-3}	4.33×10^{-3}	4.15×10^{-3}	-1.89%	-4.16%
C_F	2.88×10^{-3}	2.91×10^{-3}	-	2.90×10^{-3}	0.69%	-0.34%
C_{VP}	0.43×10^{-3}	0.48×10^{-3}	-	0.44×10^{-3}	2.33%	-8.33%
C_W	0.91×10^{-3}	-	0.92×10^{-3}	0.80×10^{-3}	-12.09%	-13.04%

4. Conclusions

The FINE™/Marine CFD code was applied to simulate the viscous flow around the DTMB 5415 hull at a relatively low Froude number, Fr = 0.248. The simulation results for the wave contours, pressure distribution, and resistance coefficients were compared with available experimental and numerical data in the literature. The wave contours predicted by FINE™/Marine agree well with the wave contours predicted in earlier numerical studies and are consistent with the experimental results. The calculated pressure distribution on the hull surface obtained in this study is in good agreement with that reported in earlier studies. Further, the calculated resistance coefficients C_T, C_F, C_{VP}, and C_W are in fairly good agreement with the experimental data and the numerical results from earlier studies. The above observations indicate that the FINE™/Marine CFD code can give a reliable and fairly accurate prediction of the flow around a ship hull at relatively low Froude numbers. Further study is recommended for the benchmark of ship resistance calculation at high Froude numbers.

Acknowledgments

This research project was partly supported by the National Research and Innovation Agency (BRIN) of the Republic of Indonesia under the Grant Penelitian Dasar Unggulan Perguruan Tinggi (PDUPT) contract no. 887/PKS/ITS/2021.

References

[1] J. L. Hess and A. M. O. Smith, "Calculation of nonlinear potential flow about arbitrary three-dimensional bodies," *Journal of Ship Research,* vol. 8, pp. 22-44, 1964.
[2] M. Insel and A. F. Molland, "An Investigation Into Resistance Components of High Speed Displacement Catamarans," *The RINA,* vol. 134, pp. 1-20, 1992.
[3] G. Jensen and H. Siding, "Rankine methods for the solution of the steady wave resistance problem," in *Proceedings 16th Symposium on Naval Hydrodynamics*, 1986, pp. 572-582.
[4] T. Li and J. Matusiak, "Simulation of modern surface ships with a wetted transom in a viscous flow," in *Proceedings of the International Offshore and Polar Engineering Conference*, 2001, vol. 4, pp. 570-576.
[5] M. Raessi, J. Mostaghimi, and M. Bussmann, "A volume-of-fluid interfacial flow solver with advected normals," *Computers and Fluids,* vol. 39, pp. 1401-1410, 2010, doi: 10.1016/j.compfluid.2010.04.010.
[6] T. Ratcliffe. 1998, Web Page http://www50.dt.navy.mil/5415/.
[7] A. Olivieri and R. Penna, "Uncertainty assessment in wave elevation measurement," in *Proceedings of the 1999 Ninth International Offshore and Polar Engineering Conference (Volume 3), Brest, France, 30 May - 4 June 1999*, 1999, vol. 7, pp. 404-411.
[8] G. Avanzini, L. Benedetti, and R. Penna, "Experimental evaluation of ship resistance for RANS code validation," *International Journal of Offshore and Polar Engineering,* vol. 10, pp. 10-18, 2000.
[9] ITTC, "7.5-03-02-02-Benchmark Database for CFD Validation for Resistance and Propulsion," *ITTC,* pp. 1-9, 2017.
[10] ITTC, "ITTC – Recommended Procedures and Guidelines - CFD, resistance and flow benchmark database for CFD validation for resistance and propulsion. 7.5-03-02-02 (revision 00)," *22nd ITTC Conference*, p. 12, 1999.
[11] DTMB 2000, Web page: http://www50.dt.navy.mil/5415/.
[12] L. Larsson, F. Stern, and V. Bertram, "Benchmarking of Computational Fluid Dynamics for Ship Flows: The Gothenburg 2000 Workshop," *Journal of Ship Research,* vol. 47, pp. 63-81, 2003. doi: 10.5957/jsr.2003.47.1.63
[13] L. Lazauskas, "Resistance and Squat of Surface Combatant DTMB Model 5415: Experiments and Predictions," 2009.
[14] R. V. Wilson, "A Technical Report by A Review of Computational Ship Hydrodynamics," 2008.
[15] Y. Ahmed and C. G. Soares, "Simulation of the Flow around the Surface Combatant DTMB Model 5415 at Different Speeds," in *13th Congress of International Maritime Association of the Mediterranean (IMAM 2009)*, 2009.
[16] Y. Ahmed, J. M. A. Fonfach, and C. Guedes Soares, "Numerical simulation for the flow around the hull of the DTMB model 5415 at different speeds," *International Review of Mechanical Engineering,* vol. 4, pp. 957-964, 2010.
[17] F. R. Menter, "Two-equation eddy-viscosity turbulence models for engineering applications," *AIAA Journal,* vol. 32, pp. 1598-1605, 1994, doi: 10.2514/3.12149.
[18] J. E. Bardina, P. G. Huang, and T. J. Coakley, "Turbulence modeling validation," in *28th Fluid Dynamics Conference*, 1997, doi: 10.2514/6.1997-2121.
[19] C. W. Hirt and B. D. Nichols, "Volume of Fluid (VOF) Method for the Dynamics of Free Boundaries," *Journal of Computational Physics,* vol. 39, pp. 201-225, 1981, doi: 10.1007/s40998-018-0069-1.
[20] P. Queutey and M. Visonneau, "An interface capturing method for free-surface hydrodynamic flows," *Computers and Fluids,* vol. 36, pp. 1481-1510, 2007, doi: 10.1016/j.compfluid.2006.11.007.

[21] Z. Li, G. Deng, P. Queutey, B. Bouscasse, G. Ducrozet, L. Gentaz, D. Le Touzé, P. Ferrant., "Comparison of wave modeling methods in CFD solvers for ocean engineering applications," *Ocean Engineering*, vol. 188, 2019, doi: 10.1016/j.oceaneng.2019.106237.
[22] Numeca International, *FINE/Marine 7.2 Theory Guide* (NUMECA online documentation platform). 2018.
[23] SIMMAN. "Workshop and Verification and Validation of Ship Manouvering Simulation Methods."
[24] Numeca International, *Theoretical Manual ISIS-CFD. NUMECA Fine/Marine; Version 6.2*. Brussels, 2017.
[25] H. K. Versteeg and W. Malalasekera, "Turbulence and its modeling," in *An Introduction to Computational Fluid Dynamics; The Finite Volume Method*, vol. 6, 2nd ed. England: Pearson Education Limited, 2007, pp. 78-78.
[26] J. D. Anderson, *Computational Fluid Dynamics; The Basic With Applications*. 1995.
[27] G. Hughes, "An analysis of ship model resistance into viscous and wave components parts I and II," in *Trans. RINA*, 1966, vol. 108, pp. 289-302, doi: 10.3233/isp-1971-1820701. [Online]. Available: https://content.iospress.com/articles/international-shipbuilding-progress/isp18-207-01
[28] C. W. Prohaska, "A simple method for the evaluation of the form factor and low-speed wave resistance," in *Proceedings of 11th ITTC, Society of Naval Architects of Japan*, 1966, pp. 65-66.
[29] I. K. Suastika, Aden, M. Indiaryanto, and B. Ali, "Prediksi nilai form factor representatif untuk kapal patroli, LST, ferry, dan tanker," in *Kumpulan Paper Terpilih di Bidang Sains dan Teknologi Kelautan-Kebumian*, I. K. A. P. Utama and M. N. Cahyadi Eds. Surabaya ITS Press, 2020, pp. 101-117.
[30] Samuel, D. J. Kim, A. Fathuddiin, and A. F. Zakki, "A Numerical Ventilation Problem on Fridsma Hull Form Using an Overset Grid System," presented at the IOP Conference Series: Materials Science and Engineering, 2021. doi: 10.1088/1757-899X/1096/1/012041.